Shock Waves (2026) 36:8
https://doi.org/10.1007/s00193-025-01259-9

ORIGINAL ARTICLE

The feasibility of high-resolution distributed acoustic sensing (HR-DAS) for measuring blast waves

J. W. Denny[1] · R. Critchley[3] · T. Lee[2] · M. Beresna[2] · G. Brambilla[2] · A. Masoudi[2]

Received: 21 March 2025 / Revised: 4 November 2025 / Accepted: 22 November 2025

Abstract
Experimental measurement of explosive blast wave overpressures is demanding, requiring specialist instrumentation that can survive extreme pressures (> 1 MPa) over short durations (< 5 ms), yet sensitive enough to resolve spatial and temporal features that vary in the mm and μs range, respectively. Distributed acoustic sensing (DAS) is an alternative approach that measures dynamic strain histories at multiple locations along a single optical fibre. This study investigates the capability of a high-resolution DAS (HR-DAS) system to capture strain responses induced by side-on (incident) blast overpressures, compared to a reference piezoelectric pressure sensor. While explosive events can produce overpressures exceeding 1 MPa, lower overpressure regimes (40–72 kPa) were adopted in this study for proof-of-concept demonstration of the HR-DAS methodology. Strain histories measured by the HR-DAS displayed reasonable qualitative agreement with overpressure histories measured using piezoelectric sensors, with the blast wave positive phase durations showing close quantitative agreement. Better correlation was observed between the measurements when HR-DAS sensors were mounted perpendicular to the blast wave propagation, validating the system's efficacy under uniform loading conditions. However, discrepancies were observed for sensors aligned parallel to the wave direction, highlighting the limitations of the spatial resolution of the HR-DAS and fibre orientation when subjected to a dynamic, spatially varying loading scenario. Findings emphasise the importance of sensor placement and configuration for distributed pressure analysis. Proof of concept results and recommendations from this study highlight an interesting opportunity for developing a novel blast pressure metrology, enabling multiple measurement points from a single optical fibre, that is small, flexible, and relatively low cost, addressing several limitations with conventional pressure instrumentation methods.

Keywords Distributed acoustic sensing · Pressure sensors · Novel instrumentation · Shock tube tests · Fibre optic sensors

1 Introduction

An explosive detonation leads to the formation of a blast wave propagating outwards at supersonic speeds. Following the detonation of a high explosive, blast wave propagation in air within an unobstructed environment theoretically exhibits a Friedlander-type [1] waveform (illustrated in Fig. 1). This idealised "side-on" blast overpressure waveform is characterised by an instantaneous pressure rise (above ambient atmospheric pressure), reaching a peak side-on overpressure, p_{so} at the time of blast wave arrival, t_A, followed by an exponential decay to ambient pressure, marking the end of the positive phase duration, t^+. Subsequently, a period of negative overpressure or "underpressure" exists before the pressure level returns to ambient atmospheric conditions, over a relatively longer negative phase duration, t.

A key objective in many blast research studies is determining the side-on overpressure history, $p_{so}(t)$, of a blast wave propagating in the air, i.e., the overpressure history measured at a surface parallel to the direction of blast wave propagation. In many blast experiments, incident (side-on) overpressures—representing the unreflected pressure of the freely propagating blast wave—are typically measured adja-

Communicated by C. Needham.

✉ J. W. Denny
Jack.Denny@soton.ac.uk

[1] School of Engineering, University of Southampton, 4011 Building 178, Burgess Road, Boldrewood Innovation Campus, Southampton SO16 7QF, UK

[2] Optoelectronics Research Centre (ORC), University of Southampton, Southampton, UK

[3] Cranfield Forensic Institute, Cranfield University, Shrivenham, UK

Published online: 12 April 2026

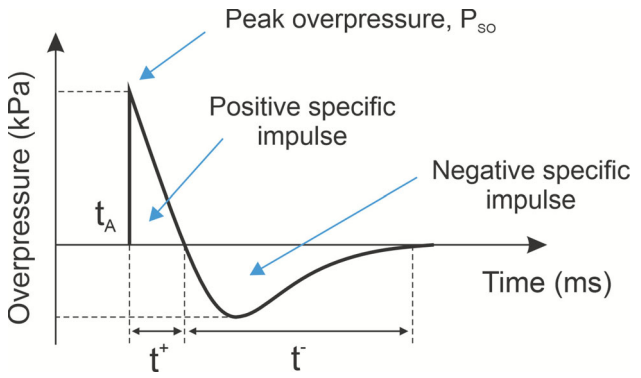

Fig. 1 Incident/side-on overpressure–time history of an idealised blast wave

cent to a target (i.e., a building, structural component, test item, biological sample, etc.) to determine the blast loading conditions and repeatability.

Experimental measurement of explosive blast overpressures is demanding, requiring specialist instrumentation that can survive extreme pressures (> 1 MPa) over short durations (< 5 ms), yet sensitive enough to resolve spatial and temporal features that vary in the mm and μs range, respectively. In the blast research community, pressure sensors [2] are traditionally used for measuring side-on overpressure histories and reflected blast pressures exerted on surfaces of the target under investigation. In shock tube experiments, for example, pressure sensors are typically flush-mounted within the inner shock tube wall to obtain side-on overpressure measurements adjacent to the target, analogous to free-field pressure measurements in explosive field tests.

However, since each sensor is high cost and requires its own high-speed data acquisition channel, only small numbers of sensors are usually deployed for experimentation, requiring strategic placement. There are also practical installation challenges; due to their size, only the sensor diaphragms that are mounted flush to the surface can be exposed to prevent local blast interaction effects (from the sensor itself) from causing spurious measurements [3].

Sensors based on optical fibre technology have demonstrated multiple performance advantages over electrical sensors for measuring blast pressures [4–7]. This includes a fast dynamic response, miniature size, lightweight, ease of installation, and immunity to electromagnetic interference. Most of these sensors are based on Fabry-Perot interferometers, which have demonstrated high accuracy under shock loading at very high sampling rates [4–7]. However, similar to piezoelectric pressure sensors, they are relatively expensive, and each sensor requires its own acquisition channel. Quasi-distributed sensors, using fibre Bragg gratings [8], can map pressure at multiple locations simultaneously, but limited sampling rates (< 20 kHz) and low strain/pressure sensitivity make them unsuitable for blast pressure measurements.

Distributed Acoustic Sensing (DAS), based on Rayleigh scattering, is an alternative sensing approach that can be used to simultaneously measure pressure-induced strain at multiple locations along a single optical fibre [9, 10]. In DAS, the optical fibre itself serves as the sensing element, where pressure-induced strain variations are spatially resolved using an optical interrogator. To spatially resolve the pressure distribution, the interrogator employs a technique known as Optical Time-Domain Reflectometry (OTDR). In OTDR, short optical pulses, in the order of tens of nanoseconds, are launched into the sensing fibre and the backscattered light is collected and analysed to map the strain distribution along the fibre [11].

Since their introduction in the early 2010s, DAS systems have been deployed in a wide range of applications. In pipeline monitoring, DAS is used to detect leaks and unauthorised activities [12]; in perimeter security, it provides intrusion detection for critical facilities such as airports and power plants [13]; in geophysical sciences, DAS offers essential insights for earthquake detection and subsurface exploration [14]; and in geotechnical engineering, it has been used for analysis of railway track behaviour [15], to name a few.

Conventional DAS systems, however, typically focus on applications that do not require high spatial resolution. The spatial resolution (or gauge length) of a DAS system is defined as the minimum distance over which the sensor output can identify a step change in strain [16]. With a typical spatial resolution of 3–5 m [13], conventional DAS systems cannot match the performance of point sensors such as electrical strain gauges or accelerometers.

To overcome this limitation, a new class of DAS systems known as High-Resolution DAS (HR-DAS) has been developed. This system enables vibration mapping at intervals as small as 10 cm [17]. It achieves this by employing a speciality optical fibre modified to reflect a small fraction of light at regular intervals (Fig. 2) [18].

Changes in strain between a given pair of reflectors can be measured by analysing the changes in the differential phases of the reflected light. For a pair of reflectors separated by distance L, the phase difference between the reflected signals at time $T = t$ is given by [17]:

$$\Delta\varphi\,(t) = \frac{4\pi n\xi}{\lambda} L \tag{1}$$

where n is the effective refractive index of the fibre, ξ is the correction factor accounting for the fibre's elasto-optic response (for a standard single-mode optical fibre (SMF-28) $\xi = 0.79$), and λ is the wavelength of the probe light. At a later time, $T = t + \Delta t$, if the distance between the reflectors

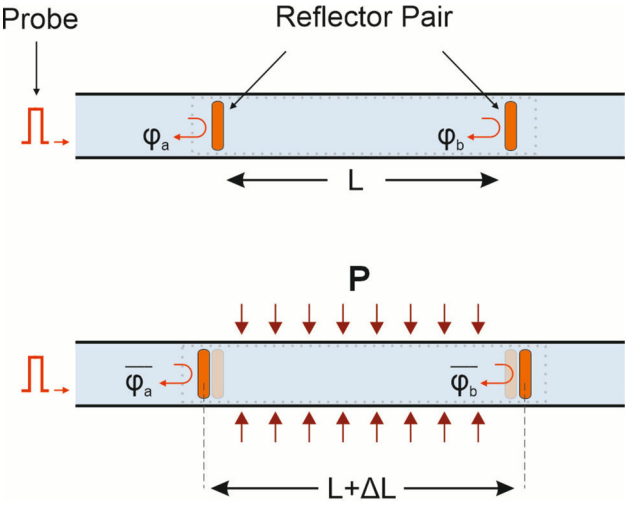

Fig. 2 The principle of High-Resolution Distributed Acoustic Sensing using speciality optical fibre. The figure illustrates a graphical representation of a fibre cross section, showing a pair of reflectors before (top) and after (bottom) elongation. These reflectors are designed to reflect a small fraction of the incident probe light. By analysing the phases of the back-reflected light, changes in the distance between the two reflectors can be tracked with nano-strain accuracy

changes by ΔL, the phase difference becomes:

$$\Delta\varphi\,(t+\Delta t) = \frac{4\pi n\xi}{\lambda}\,(L+\Delta L) \tag{2}$$

The resulting change in phase, and therefore the strain-induced elongation, is obtained by subtracting (1) from (2):

$$\Delta\Phi = \Delta\varphi\,(t+\Delta t) - \Delta\varphi\,(t) = \frac{4\pi n\xi}{\lambda}\Delta L \tag{3}$$

By launching probe pulses into the fibre at regular intervals, Δt, and measuring the changes in the phase difference over time, variations in fibre length can be spatially resolved with nano-strain accuracy.

Thus far, HR-DAS has been applied as an array of strain gauges for studies such as wave propagation in solids and structural analysis of bridges. However, its feasibility and performance for measuring pressure-induced strain under highly dynamic blast loading have yet to be evaluated. With ongoing improvements reducing the effective gauge length from 15 cm towards 1 cm, comparable to the active diameter of typical piezoelectric pressure sensors, HR-DAS presents a compelling opportunity for high-resolution, distributed blast measurements. Such capability could overcome the limitations of current instrumentation in the field, enabling blast pressure measurements at thousands of locations using a single fibre. In addition, HR-DAS systems offer several practical advantages, including cost-effectiveness, lightweight design, flexible installation, and immunity to electrical interference.

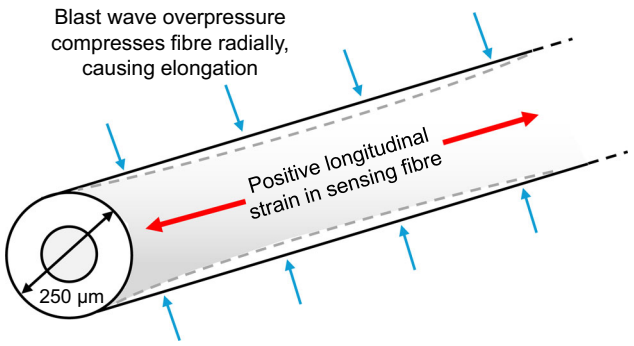

Fig. 3 Schematic illustrating how blast-pressure-induced radial strain induces longitudinal fibre strain, interrogated by the HR-DAS

1.1 Study hypothesis

For the proof-of-concept study, it was hypothesised that the air blast overpressure would radially compress the fibre, inducing axial elongation and corresponding strain which could be detected by the HR-DAS setup as an indirect way to measure air blast parameters (Fig. 3). Conversely, it was also anticipated that the underpressure phase of a blast wave would cause radial fibre expansion and thus, longitudinal contraction of the sensing fibre, enabling measurement of negative strains.

The relationship between external pressure and axial strain in the fibre is analogous to that described by Barlow's formula for thin-walled pipes, where radial loading induces longitudinal strain. In this study, external blast pressure applied to the fibre surface is expected to generate axial strain along its length, supporting the hypothesis that blast loading can produce a measurable response in the sensing fibre.

The sensitivity of a bare silica optical fibre to hydrostatic pressure is given by [19]:

$$\frac{\Delta\varphi}{PL} = -\frac{\beta\,(1-2\mu)}{E} + \frac{\beta n^2}{E}\,(1-2\mu)\,(2p_{12}+p_{11}) \tag{4}$$

where $\Delta\varphi$ is the pressure-induced phase change, P is the hydrostatic pressure, L is the fibre length, β is the propagation constant, μ is the Poisson's ratio, E is the Young's modulus, and p_{12} and p_{11} are strain-optic coefficients. Substituting the parameters for silica fibre interrogated by a 1550-nm laser into (4) yields:

$$\begin{aligned}\frac{\Delta\varphi}{PL} &= -5.57\times10^{-5} + 3.92\times10^{-5}\\ &= -1.65\times10^{-5}\,\frac{\text{rad}}{\text{Pa m}}\end{aligned} \tag{5}$$

This theoretical calculation indicates that, for the phase difference between the two reflectors, 15 cm apart, to shift by π

radians, the pressure on the fibre between the reflectors must increase by:

$$\frac{\pi}{1.65 \times 10^{-5} \times 0.15} = 1.26\,\text{MPa} \tag{6}$$

It is important to note that this 1.26 MPa value represents a theoretical upper limit for pressure measurement, assuming uniform hydrostatic loading. In practice, the actual safe operating pressure is expected to be lower due to non-uniform pressure distribution, partial fibre exposure, and mounting constraints.

Interestingly, previous studies have shown that applying polymer coatings to optical fibres can enhance pressure sensitivity by up to 38 times [20]. To assess the pressure sensitivity of the fibre used in this study's shock tube tests, an optical interferometer, similar to that used in [19], was used along with an underwater speaker in a water tank. The experimental results on the acrylate-coated optical fibre showed a hydrostatic pressure sensitivity of:

$$\frac{\Delta\varphi}{PL} = -7.45 \times 10^{-5}\ \frac{\text{rad}}{\text{Pa m}} \tag{7}$$

This paper reports novel experimental findings that examine the viability of using HR-DAS as an instrumentation method for measuring free-field blast wave parameters (i.e., unobstructed propagation of a blast wave in the absence of any reflecting surfaces or obstacles).

2 Methodology

2.1 Overview

A total of 11 shock tube tests were undertaken at Cranfield University, Shrivenham Defence Academy, to evaluate the feasibility and performance of the novel HR-DAS sensor system for measuring blast pressure-induced strain histories, with measurements compared against a reference piezoelectric pressure transducer.

The gas-driven shock tube (full details available in [21]) was used to generate near-planar blast waves in the driven section following the rupture of the diaphragm, which separates the driver section, containing compressed air (Fig. 4). The tube has an internal diameter of 565 mm, with a 4000-mm driven section and a 500-mm driver section when separated by a diaphragm. Shock tube diaphragms were composed of Mylar sheet membranes (supplied by CFS Mylar Supplies, UK) secured by rubber gaskets. Two diaphragm thicknesses, 125 µm and 250 µm, were used to generate two distinct low-level blast loading conditions that remained within the safe operating limits of the indoor shock tube facility. The thicker

Fig. 4 Photograph of the shock tube at Cranfield University, UK, showing the full experimental arrangement and overall scale. The internal sensing fibre, secured to the inner tube wall with masking tape, is also visible

250 µm diaphragms required a higher driver pressure to rupture, resulting in a stronger incident shock wave. The driver chamber was pressurised using ambient air supplied from a nearby compressor system until diaphragm rupture, at mean pressures of 102 ± 3 kPa and 198 ± 5 kPa for the 125 µm and 250 µm Mylar membrane thicknesses, respectively.

Side-on blast overpressure histories were measured at the shock tube inner wall surface by both the HR-DAS sensor system and a piezoelectric sensor at 200 mm from the shock tube exit (Fig. 4). For all tests, a Kistler 603B 0-200 bar piezoelectric pressure sensor was flush-mounted within the inner shock tube wall at 200 mm from the end of the shock tube exit to obtain side-on overpressure measurements. A 35-mm piezoelectric sounder sensor trigger drum disc was mounted adjacent to the piezoelectric pressure sensor to trigger and initiate the Imatek®C3008 general purpose Data Acquisition System, coupled with a Kistler®5017B microprocessor-controlled multi-channel charge amplifier. Data was sampled at a rate of 3 MHz over a time duration of 100 ms, where a pre-trigger of 30 ms was used to ensure full capture of the loading event.

The HR-DAS was used to interrogate a single fibre, comprising multiple sensors, which was secured to the inner shock tube wall. The fibre was secured to the shock tube wall using double-sided Sellotape, with an overlying layer of masking or duct tape to secure it in place. Polyethylene-coated duct tape was selected for Phase B tests as it provided improved adhesion and resistance to delamination from the blast wave compared to the masking tape used in Phase A. This change was based on practical observations during early testing and aimed to improve fibre retention during repeated blast events.

Table 1 Summary of experimental tests and variables examined

Testing phase	No. of tests	Shock tube diaphragms	Piezoelectric sensor arrangement	HR-DAS sensor arrangement	No. of pressure datasets	No. of HR-DAS datasets
A	7	125 μm (×5) 250 μm (×2) Mylar diaphragms	One flush-mounted at 200 mm from the shock tube exit	Three optical fibre sensing channels. All arranged in a "hoop" configuration. Double-sided tape with masking tape covering	7	2
B	4	125 μm Mylar diaphragms	One flush-mounted at 200 mm from the shock tube exit	Four optical fibre sensing channels. Two are arranged in "hoop" configuration and two in "longitudinal" configuration. Double-sided tape with duct tape covering	4	3

"Flush-mounted" refers to the piezoelectric pressure gauges. HR-DAS fibres were surface-mounted using adhesive tape, as described in Sect. 2.2

At HR-DAS sensing locations (in between reflectors), the fibre was manually pre-strained during installation by applying gentle axial tension prior to securing. Pre-straining was used to ensure that the fibre remained under tension throughout the entire blast event. During the blast wave positive phase duration, the fibre experiences additional tensile strain, while during the negative phase, the strain is reduced but remains above zero, preventing any slack or buckling. While the level of pre-strain may have varied slightly between sensing locations, this is not expected to have influenced the measurements significantly, as the HR-DAS system captures relative changes in strain rather than absolute values. Due to the fibre's small diameter (i.e., 250 μm), it was positioned almost flush with the inner wall of the shock tube. Hence, the effect of reflected pressure from the fibre was assumed to be negligible. As the fibres were secured directly to the shock tube wall, the system also responds to structural vibration or wall strain induced by the blast loading. This potential coupling effect is examined further in the discussion.

Two orientations of DAS sensor placement were examined, including "hoop" placement, where the sensing elements were secured in the circumferential direction at a fixed distance of 200 mm from the shock tube exit, and "longitudinal" placement, where the sensing fibre was orientated parallel to the shock tube's longitudinal axis. Experiments were undertaken in two phases, examining two DAS placement orientations, summarised in Table 1, and described as follows:

Phase A—Three DAS sensors in series. This phase explored only the hoop sensor placement and two blast loading magnitudes. The DAS sensors were adhered using double-sided tape (≈ 0.1 mm thick) topped with 3 M™101E crepe paper masking tape (0.12 mm thick) (Fig. 5).

Phase B—Four DAS sensors in series. This phase explored both hoop and longitudinal fibre placement with respect to the inner shock tube wall, considering one loading condition. The DAS sensors were adhered using double-sided tape (≈ 0.1 mm thick) topped with RS PRO high tack duct tape (0.17 mm thick) (Fig. 6).

2.2 HR-DAS setup

Figure 7 shows the block diagram of the sensing arrangement on the left and a photo of the HR-DAS interrogator on the right. The optical interrogator comprised a pulse synthesiser arm and a receiver arm. The pulse synthesiser arm consisted of a narrow linewidth seed source ($\lambda = 1550$ nm, $\Delta\nu = 2$ kHz) that was externally modulated by an electro-optic modulator (EOM) to generate 1-ns probe pulses. A 1-ns pulse corresponds to a pulse duration of 20 cm. A wavelength of 1550 nm is commonly used in distributed optical fibre sensors since silica optical fibre has the lowest attenuation at this wavelength. Using this wavelength allows the sensing range to be maximised. The probe pulses were launched into the sensing fibre, and the reflected lights were redirected into the receiving arm of the optical interrogator via circulator C.

The sensing fibre was fabricated using an automated reel-to-reel fibre inscription setup [17]. A standard ITU-T G.652 single-mode silica fibre with a 125-μm cladding and 250-μm acrylate protective coating was used as the feed fibre. Using the inscription setup, multiple reflector pairs were written into the core of the fibre, each with an average reflectance of −56 dB. The reflectors within each pair were separated by 15 cm, while the spacing between reflector pairs was 20 cm. A 10-m length of standard G.652 fibre was used to connect the sensing fibre to the HR-DAS interrogator. The interrogator was housed in an adjacent room to isolate it from the shock tube facility. For the single fibre, each pair of reflectors therefore provided a series of fibre sensing lengths of 15 cm (with 20 cm spacings), which were denoted by unique channel numbers within the experimental setup (Fig. 5).

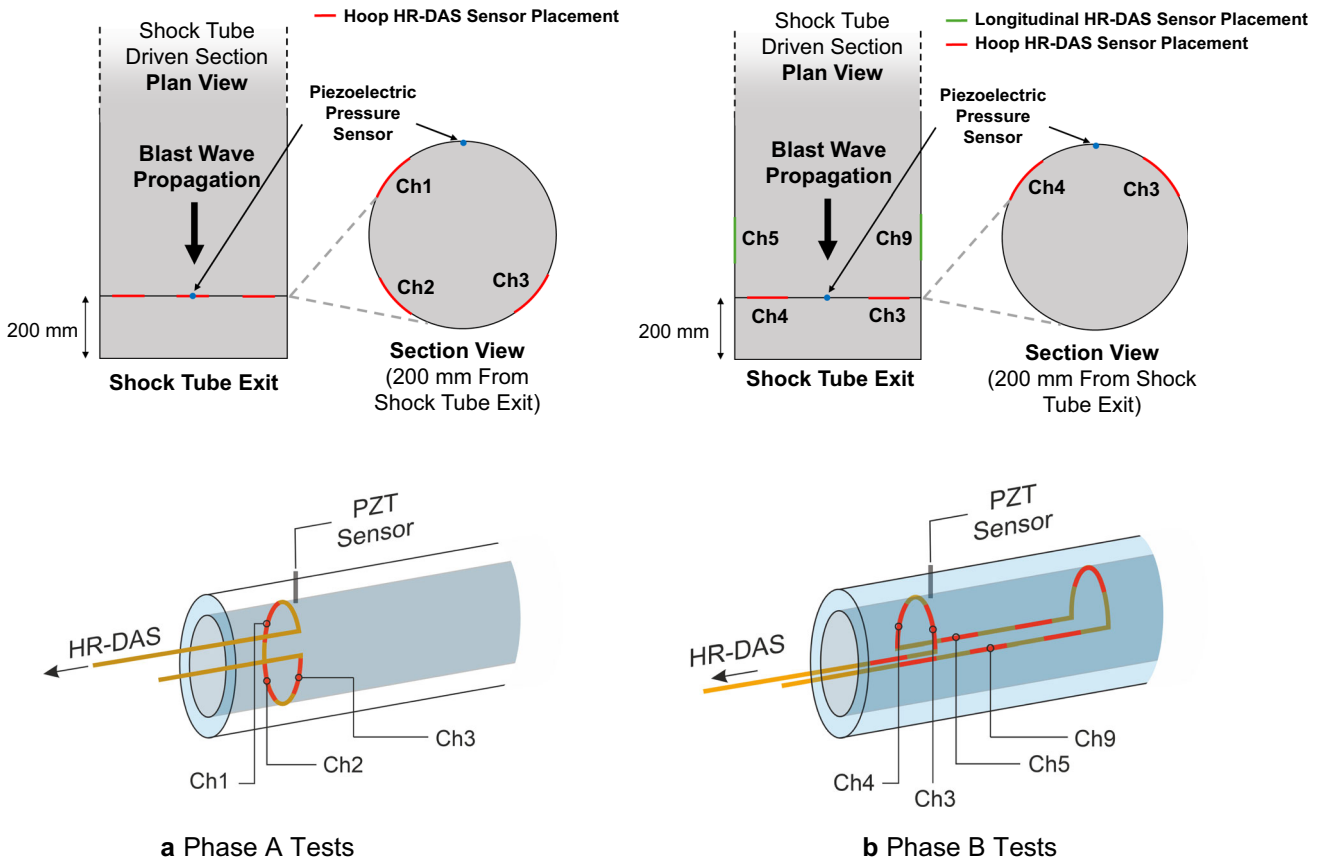

Fig. 5 Plan, section, and isometric schematics of experimental setup and sensor arrangements

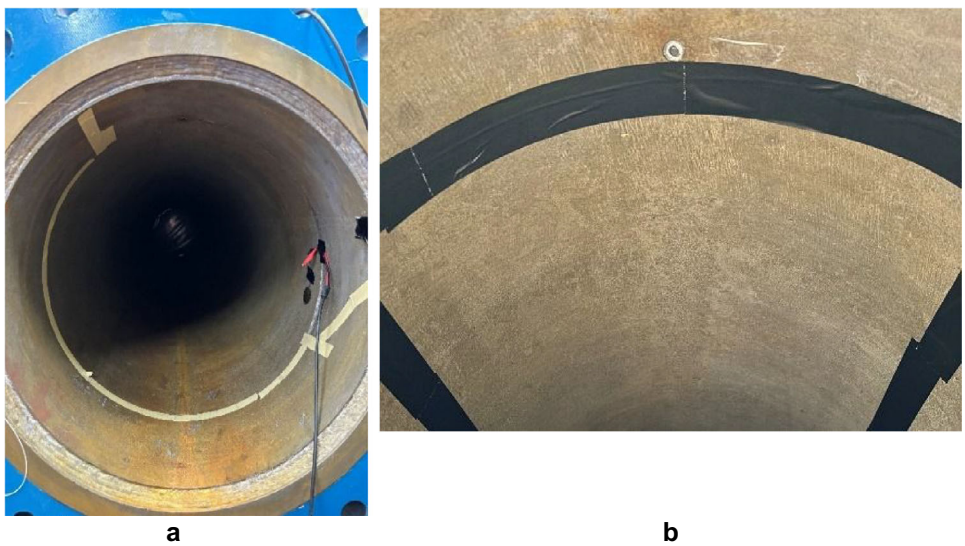

Fig. 6 Photos of the arrangement of instrumentation secured to the inner shock tube wall. **a** Phase A: HR-DAS arrangement on the inner shock tube wall showing "hoop" placement with masking tape covering. **b** Phase B: HR-DAS arrangement on the inner shock tube wall showing both "hoop" and "longitudinal" placements with electrical insulation tape covering

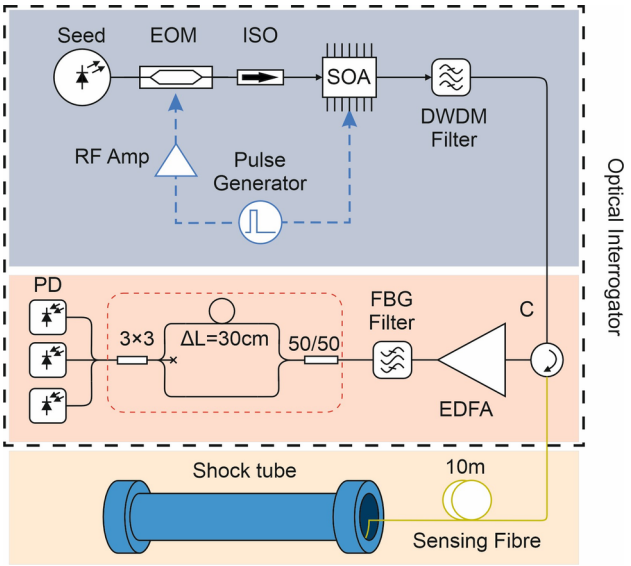

Fig. 7 The block diagram of the test arrangement and the HR-DAS optical interrogator

At the receiving arm of the HR-DAS interrogator, the backscattered signal from the sensing fibre was first amplified by an Erbium-doped optical amplifier and then filtered by an FBG filter ($\lambda B = 1550.1\,\text{nm}$, $\Delta\lambda = 0.2\,\text{nm}$, reflectivity = 99%) to minimise the noise from the optical amplifier. The amplified back-reflected light was then passed through a Mach–Zehnder Interferometer with a 30-cm path imbalance to mix the back-reflected signals from the reflectors in each reflector pair. Finally, the mixed signal at the output of the interferometer was detected by three amplified photodetectors (BW = 500 MHz, TIA = 100 kΩ (MenloSystems-FPD610)) and sampled with a 700-MHz bandwidth PCIe digitiser at a rate of 1 GS/s.

2.3 HR-DAS data acquisition

The pulse repetition rate of the HR-DAS was set to 500 kHz, which means that each reflector pair was sampled once every 2 µs. For a blast wave with a positive phase duration of approximately $t^+ = 2.8\,\text{ms}$, the interrogator recorded 1400 data points.

The HR-DAS system used in this study lacked an event-triggered input, so data acquisition was initiated manually approximately two seconds before the diaphragm's expected failure, based on the user's knowledge of the approximate diaphragm rupture pressures. Due to the high pulse repetition rate (the system was set to record 500 sensing nodes each at 500 kHz, including the additional fibre used to connect the interrogator to the fibre on the shock tube), the interrogator could record a maximum of 8 s of data per initiation.

2.4 Data post-processing

As the piezoelectric data acquisition and the HR-DAS system were not synchronised during testing, pressure histories (captured by the piezoelectric sensor) and strain histories (from HR-DAS) were time-shifted based on the rising edge of the shock wave to have a common arrival time of $t_A = 10\,\text{ms}$, recorded by both systems. The alignment was performed manually in post-processing by visually identifying the sharp rise associated with shock arrival in both datasets and shifting the HR-DAS traces accordingly. This procedure was applied uniformly across all tests to provide a common reference point for comparison. The time shift was used solely to enable visual comparison of waveform shape and duration and does not represent a synchronised or physically meaningful time of arrival. This post-processing was considered acceptable to enable comparison between respective pressure and strain-time histories and to examine test-to-test repeatability.

All HR-DAS strain-time histories were manually inspected to identify the blast wave event within the recorded data (Fig. 8). Through inspection of the HR-DAS strain histories over a wider time period (Fig. 8a), the arrival of the shock wave (Fig. 8b) could be clearly identified following an initially undisturbed period. The shock front arrival was characterised by a distinct rise in strain (Fig. 8a), followed by multiple oscillations, representing the vibration of the shock tube.

All DAS strain data were filtered using a Butterworth bandpass filter with a lower cutoff frequency of 10 Hz and a higher cutoff frequency of 240 kHz. The upper value represents the Nyquist limit (500 kS/s gives the maximum frequency of 250 kHz), while the lower cutoff frequency was set to remove any temperature effects on the fibre without altering the waveform.

3 Results

3.1 Phase A results

3.1.1 Piezoelectric pressure sensor results

Blast wave parameters measured using the piezoelectric pressure sensor exhibited a Friedlander-type profile, characterised by a near-instantaneous pressure rise followed by an exponential decay (Fig. 9). For both loading conditions, a clear negative phase was observed, returning to ambient pressure before the arrival of a second blast wave.

The 125-µm Mylar diaphragms generated a mean peak side-on overpressure of $p_{so,av} = 47.1\,\text{kPa}$ across five tests (Fig. 9a), with a mean positive phase duration of $t^+ = 2.88\,\text{ms}$ (Table 2). The 250-µm Mylar diaphragms generated higher side-on overpressures, with a mean of 71.9 kPa

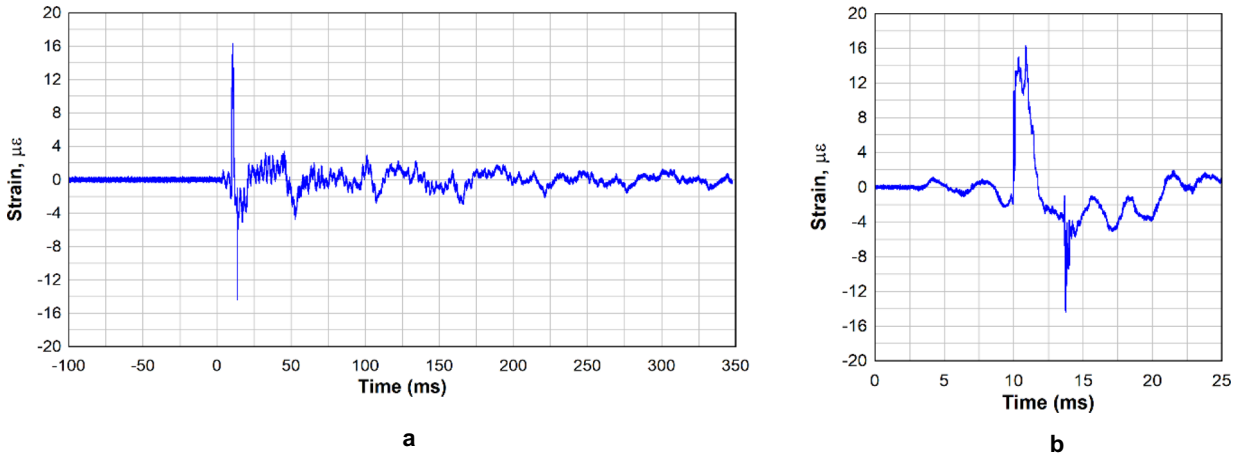

Fig. 8 Identifying the blast wave within the HR-DAS strain-time histories. **a** Extended time domain showing clear shock wave arrival (Ch4; Test 31). **b** Reduced time domain showing shock wave arrival (Ch4; Test 31)

across two tests (Fig. 9b) and a slightly longer duration of $t^+ = 3.17$ ms (Table 3). Piezoelectric pressure measurements demonstrated very good repeatability across all tests; therefore, the HR-DAS system can be assumed to have been subjected to repeatable loading conditions in each test. Blast parameters in Tables 2 and 3 were extracted by manual inspection of the raw pressure–time histories. Peak incident overpressure was taken as the maximum value immediately following shock arrival. In cases where a secondary rise exceeded this value, the maximum overpressure was recorded separately. As no filtering was applied, some variation due to high-frequency noise may be present.

3.1.2 HR-DAS results

HR-DAS strain data was captured for one test for each loading condition (i.e., using the 125-μm and 250-μm Mylar diaphragms) due to the challenges of manual data triggering. Data from fibre sensing channels 1 (Ch1) and 3 (Ch3) were successfully captured in both tests (Table 4), with channel 2 ignored due to spurious readings.

Strain histories are overlaid with overpressure histories (from the piezoelectric transducer) in Fig. 10, with arrival times shifted to $t_A = 10$ ms. Reasonable qualitative agreement is observed between the pressure profiles measured using the piezoelectric sensor and the strain-time history measured by the HR-DAS system. In both tests, blast wave arrival was characterised by an instantaneous rise in strain, followed by decay and a period of negative strain, analogous to the underpressure phase of the blast pressure profile (Fig. 10). Beyond this, strain histories exhibited significant oscillations, which may reflect movement of the masking tape covering the sensing fibre.

Peak strains of 5.22 με and 6.60 με were measured from Ch1 and Ch3, respectively, during shock wave arrival when

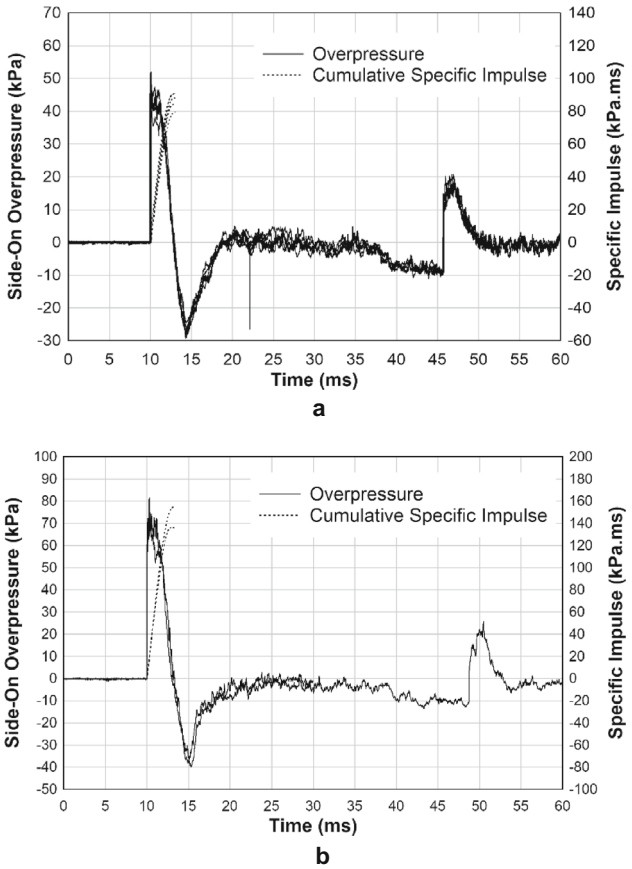

Fig. 9 Overlaid side-on overpressure and cumulative impulse histories measured by the piezoelectric pressure sensor. **a** Measured blast wave using 125-μm Mylar diaphragm membrane. **b** Measured blast wave using 250-μm Mylar diaphragm membrane

subjected to blast loading using the 125-μm Mylar membrane. Peak strains of 11.78 με and 12.50 με were measured at Ch1 and Ch3, respectively, when subjected to blast loading

Table 2 Blast wave parameters measured by the piezoelectric sensor using 125-μm diaphragms in shock tube

Test ID	Peak side-on overpressure (kPa)	Maximum overpressure (kPa)	Specific impulse (kPa ms)	Positive phase duration (ms)	Peak (negative) underpressure (kPa)	Negative phase duration (ms)
21	40.5	40.5	79.4	2.95	−24.5	6.37
22	51.8	51.8	90.4	2.93	−28.2	6.81
23	52.0	52.0	90.8	2.91	−27.6	5.70
25*	44.9	44.9	84.2	2.78	−29.1	5.81
27	46.5	46.5	88.2	2.82	−26.8	5.79
Mean	47.1	47.1	86.6	2.88	−27.2	6.10
S.D.	4.4	4.4	4.3	0.07	1.6	0.43

*Denotes tests where HR-DAS data was successfully captured

Table 3 Blast wave parameters measured by the piezoelectric sensor using 250-μm diaphragms in shock tube

Test ID	Peak side-on overpressure (kPa)	Maximum overpressure (kPa)	Specific impulse (kPa ms)	Positive phase duration (ms)	Peak (negative) underpressure (kPa)	Negative phase duration (ms)
26	71.5	71.5	136.6	3.04	−38.3	12.31
28*	72.3	81.6	154.8	3.30	−40.1	13.67
Mean	71.9	76.6	145.7	3.17	−39.2	12.99
S.D.	0.4	5.1	9.1	0.13	0.9	0.68

*Denotes tests where HR-DAS data was successfully captured

Table 4 Strain data captured by HR-DAS sensors subjected to shock waves using 125-μm and 250-μm Mylar diaphragms (Phase A)

Test ID	Shock tube blast loading setup	HR-DAS channel no.	HR-DAS measurements				
			Peak incident strain (με)	Maximum strain (με)	Positive phase duration (ms)	Peak negative strain (με)	Negative phase duration (ms)
25	125-μm Mylar membrane ($p_{so} \approx 45$ kPa)	1	5.22	5.22	2.77	−9.96	4.07
		2	–	–	–	–	–
		3	6.60	6.60	2.20	–	–
28	250-μm Mylar membrane ($p_{so} \approx 72$ kPa)	1	11.78	11.78	2.20	−10.19	3.45
		2	–	–	–	–	–
		3	12.50	12.50	1.69	−18.70	4.60

utilising the 250-μm Mylar membrane (Table 4). The approximate doubling of peak strain values is consistent with the increase in maximum overpressure (i.e., $p_{so,max} = 44.9$ kPa and $p_{so,max} = 81.6$ kPa), which further validates the identification of the blast wave within the strain histories measured by the HR-DAS setup. This also confirms that strains measured by the HR-DAS are proportional to the applied blast wave overpressure, indicating suitability and potential as a blast instrumentation tool. This proportional relationship is expected since, under elastic conditions, the circumferential and axial strains induced in a thin-walled cylindrical structure are approximately linear with the applied external pressure, provided the geometry, material stiffness, and boundary conditions remain constant between tests.

Some inconsistencies were observed for the DAS measurements during the negative "underpressure" phase. Peak negative strains of −9.96 με (Ch1), −10.19 με (Ch1), and −18.70 με (Ch3), measured during tests 25 and 28 (Table 4), are larger in magnitude than peak strains from the positive phase, inconsistent with piezo pressure measurements. This suggests that sensing fibres experienced a relatively higher level of negative strain when subjected to negative blast

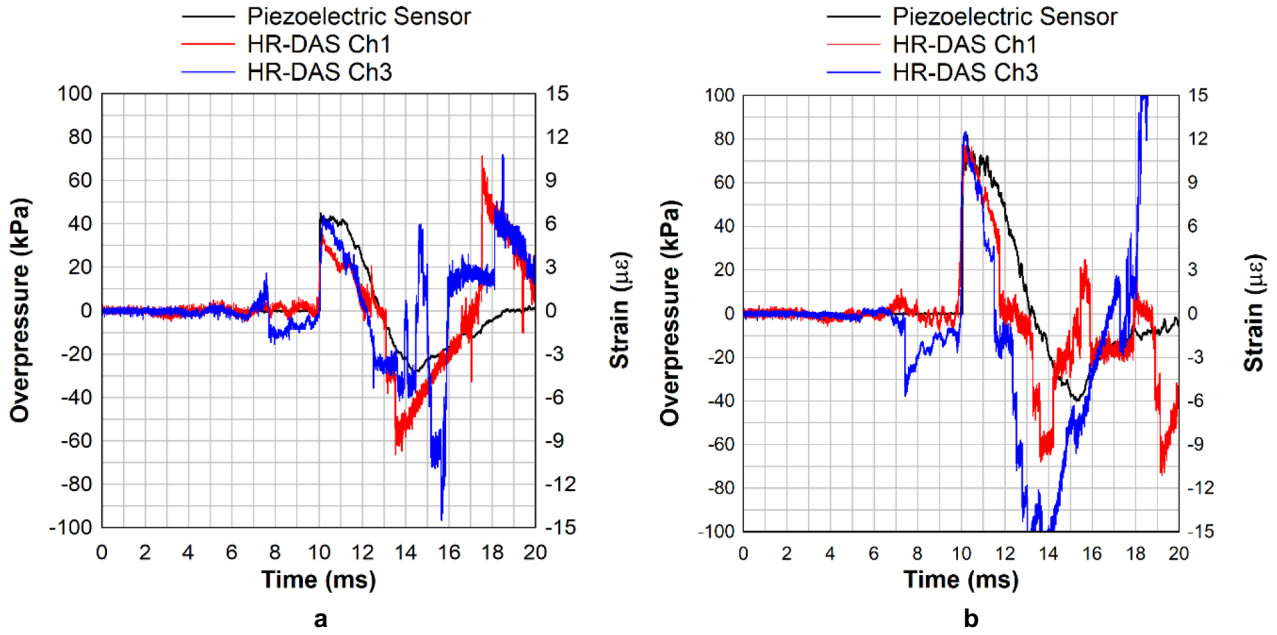

Fig. 10 Overlaid overpressure and strain histories measured by the piezoelectric transducer and HR-DAS sensors. **a** Test no. 25: 125-μm Mylar, i.e., $p_{so} = 45$ kPa. **b** Test no. 28: 250-μm Mylar, i.e., $p_{so} = 72$ kPa

overpressure, when the fibre theoretically experiences radial expansion.

In Table 3, agreement of the positive and negative phase time durations is assessed between measurements using the piezoelectric sensor and HR-DAS. Comparably better agreement was observed for the test at lower overpressure ($p_{so} = 45$ kPa), with durations measured by the DAS system slightly lower than measured by the piezo sensor by −0.01 ms (−0.4%) and −0.58 ms (−20.9%) for the positive phase (Table 5). Negative phase durations were more noticeably underpredicted by the HR-DAS sensors by −1.74 ms (−29.9%) in test 25 ($p_{so} = 45$ kPa), and by −10.22 ms and −9.07 ms (−74.8% and −66.3%) in test 28 ($p_{so} = 72$ kPa) (Table 5). These inconsistencies (magnitude and duration of strains during the negative phase in comparison with piezo measurements) may suggest that the HR-DAS sensors are less suited to measuring underpressure experienced during the blast negative phase.

3.1.3 Limitations of Phase A measurements

The primary issue identified after the Phase A tests was the influence of the masking tape. By the end of the test series, visual inspection revealed clear signs of the masking tape lifting during this phase. This suggests that the low adhesion between the tape and the shock tube likely caused both the tape and, consequently, the fibre to lift during testing. This would have introduced spurious strain readings, particularly during the negative pressure phase.

3.2 Phase B results

3.2.1 Piezoelectric pressure sensor results

Similar to Phase A tests, blast wave parameters measured using the piezoelectric pressure sensor during Phase B exhibited a Friedlander-type pressure profile, characterised by a near-instantaneous pressure rise followed by an exponential decay (Fig. 11). The 125-μm Mylar diaphragms generated a mean peak side-on overpressure of $p_{so,av} = 39.4$ kPa across four tests, with a mean positive phase duration of $t^+ = 2.76$ ms (Table 6). Similar to Phase A, a clear negative phase was observed, returning to ambient pressure before the arrival of a second blast wave, and very good repeatability was observed across all tests (Table 6). It is therefore assumed that the HR-DAS system was subjected to consistent blast loading across all tests.

3.2.2 HR-DAS results

HR-DAS strain data were successfully captured for three of the four tests and summarised in Table 7 for channels 3 and 4. Initial inspection of the data demonstrated clear agreement between the HR-DAS strain history and pressure profile (Fig. 12), both in terms of waveform and respective durations throughout the positive and negative phases, including the arrival of the second blast wave at $t = 45$ ms.

The HR-DAS trace comprises two components: (1) strain induced by the pressure of the blast wave, and (2) strain transmitted mechanically through coupling between the fibre and

Table 5 The comparison of positive and negative blast wave durations measured by the piezoelectric and HR-DAS sensors (Phase A)

Test ID	DAS channel no.	Shock tube blast loading setup	HR-DAS positive phase duration (ms)	Piezoelectric positive phase duration (ms)	Difference (ms)	% Difference	HR-DAS negative phase duration (ms)	Piezoelectric negative phase duration (ms)	Difference (ms)	% Difference
25	1	125 µm ($p_{so} \approx 45$ kPa)	2.77	2.78	−0.01	−0.4%	4.07	5.81	−1.74	−29.9%
	2		–		–	–	–		–	–
	3		2.20		−0.58	−20.9%	–		–	–
28	1	250 µm ($p_{so} \approx 72$ kPa)	2.20		−1.10	33.3%	3.45		−10.22	−74.8%
	2		–	3.30	–	–	–	13.67	–	–
	3		1.69		−1.61	48.8%	4.60		−9.07	−66.3%

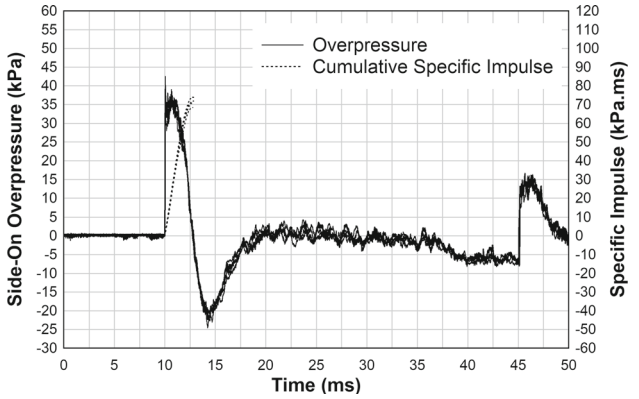

Fig. 11 Overlaid side-on overpressure and cumulative specific impulse histories measured by the piezoelectric pressure sensor

the shock tube wall. This effect is evident in Fig. 12, where oscillations begin approximately 7.5 ms before the arrival of the main shock front. Given that sound propagates nearly 20 times faster in steel than in air, these early oscillations are attributed to mechanical waves travelling along the shock tube wall and reflecting from its boundaries. The relatively constant amplitude and frequency of these oscillations further support this interpretation.

Data from channels 3 and 4 (Ch3 and Ch4), where the sensing fibres were configured in a hoop arrangement, are overlaid with overpressure histories (from the piezotransducer) in Fig. 13, with waveforms time-shifted to $t_A = 10$ ms. Across the three tests, generally, good qualitative agreement is observed between the HR-DAS strain histories measured at channels 3 and 4 and the piezoelectric pressure profiles (Fig. 13). Similar to Phase A, blast wave arrival was characterised by an instantaneous rise in strain for both channels, followed by decay and a period of negative strain, corresponding to the underpressure phase of the blast wave (Fig. 13). Despite good correlation for the positive phase, in tests 32 and 34, channel 4 exhibited a spurious second peak in positive strain. The deterioration in the HR-DAS data from test #31 to test #34 can be associated with the degradation of the bond between the fibre and the shock tube. Inspection of the electrical insulation tape, used to secure the fibre to the tube, revealed signs of detachment at the end of the testing, highlighting the importance of selecting a more reliable adhesive for securing the fibre inside the tube for future tests.

Peak positive strains ranged from 22.9–25.2 µε and 14.8–24.3 µε at Ch3 and Ch4, respectively (Table 7), when subjected to repeat shock tube loading using the 125-µm Mylar membrane (i.e., $p_{so,average} = 39.4$ kPa). In comparison to Phase A, using the same diaphragm thickness (and similar overpressure), peak positive strains in Phase B were approximately a factor of three higher. Given that the blast wave overpressure levels remained similar between both

Table 6 Summary of blast wave parameters measured by the piezoelectric sensor using 125-μm Mylar diaphragms

Test ID	Peak side-on overpressure (kPa)	Specific impulse (kPa ms)	Positive phase duration (ms)	Peak (negative) underpressure (kPa)	Negative phase duration (ms)
31*	38.1	70.9	2.71	−21.8	6.12
32*	42.5	73.9	2.78	−24.6	5.77
33	37.7	68.5	2.71	−20.5	6.12
34*	39.1	71.8	2.84	−22.3	6.99
Mean	39.4	71.3	2.76	−22.3	6.25
S.D.	1.9	1.9	0.05	1.5	0.45

* Denotes tests where HR-DAS data was successfully captured

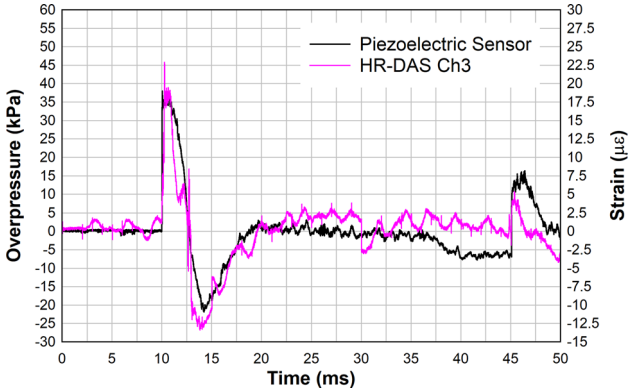

Fig. 12 Good qualitative agreement between the overpressure and strain history measured by the piezoelectric transducer and HR-DAS sensor (Ch3) in hoop configuration (Test 31)

phases, the increased (positive) strain magnitudes in Phase B may be attributed to the electric insulation tape covering.

Peak negative strains ranged between −10.5 to −20.7 με in Phase B tests (Table 7), with magnitudes typically less than strains during the positive phase, demonstrating better agreement with the piezo pressure measurements than found in Phase A tests. This indicates that the sensing fibres experienced peak strain magnitudes (positive and negative) that were more closely aligned with the distribution of max/min overpressures.

In Table 8, time durations are compared between the piezoelectric transducer and HR-DAS sensor measurements. Fair agreement was observed during the positive phase, although durations measured by the HR-DAS system were generally lower than the piezo sensor pressure trace by between −12.7% and −23.4% (Table 6). The duration of negative strain measured by the HR-DAS sensors demonstrated relatively less agreement with the corresponding pressure durations, which were longer by 14.9–47.7% (Table 8).

HR-DAS sensors in the longitudinal arrangement demonstrated generally poor agreement with piezo sensor pressures (Fig. 13 right). For this sensor arrangement, strain-time histories did not have an instantaneous rise (analogous to the shock wave pressure history), but instead, exhibited a gradual decrease and increase in strain. Similarly, both the positive and negative strain phase durations did not show agreement with the overpressure durations. The initial (negative) strain response (Fig. 13 right) occurred for a longer duration than the side-on overpressure history. Peak positive and negative strain values were also approximately 2–3 times larger than those measured by sensing fibres in the hoop orientation. While beyond the scope of the study, these results highlight the importance of DAS sensor orientation with respect to the propagation of the shock wave.

4 Discussion

Overall, this study has confirmed the feasibility of using HR-DAS for indirectly measuring side-on blast wave parameters in air, verified through qualitative agreement with pressure measurements obtained by a reference piezoelectric pressure sensor. Qualitative agreement included both an instantaneous rise in positive strain followed by a decay and negative strain phase, and even the second blast wavefront, analogous to the reference overpressure waveforms, thus confirming our hypothesis. The temporal behaviour of HR-DAS strain histories was quantitatively assessed through comparisons with reference overpressure histories, confirming reasonable agreement with the timing (generally within 20%) and waveform for the positive phase durations. In contrast, the interpretation of the subsequent negative strain phase is less certain. While the response is consistent with the expected underpressure phase of a Friedlander waveform, it may also reflect structural vibration or mechanical relaxation effects following the initial loading.

Two different loading magnitudes (i.e., $p_{so} \approx 47$ kPa and 72 kPa) were examined in Phase A, with peak strain observed to approximately double, consistent with the peak blast wave overpressure. While this suggests blast overpressure and induced fibre strain are proportional, the performance of HR-DAS should be investigated over a wider range of blast overpressures and durations, plus examine the potential effects of the fibre material's strain sensitivity. At higher

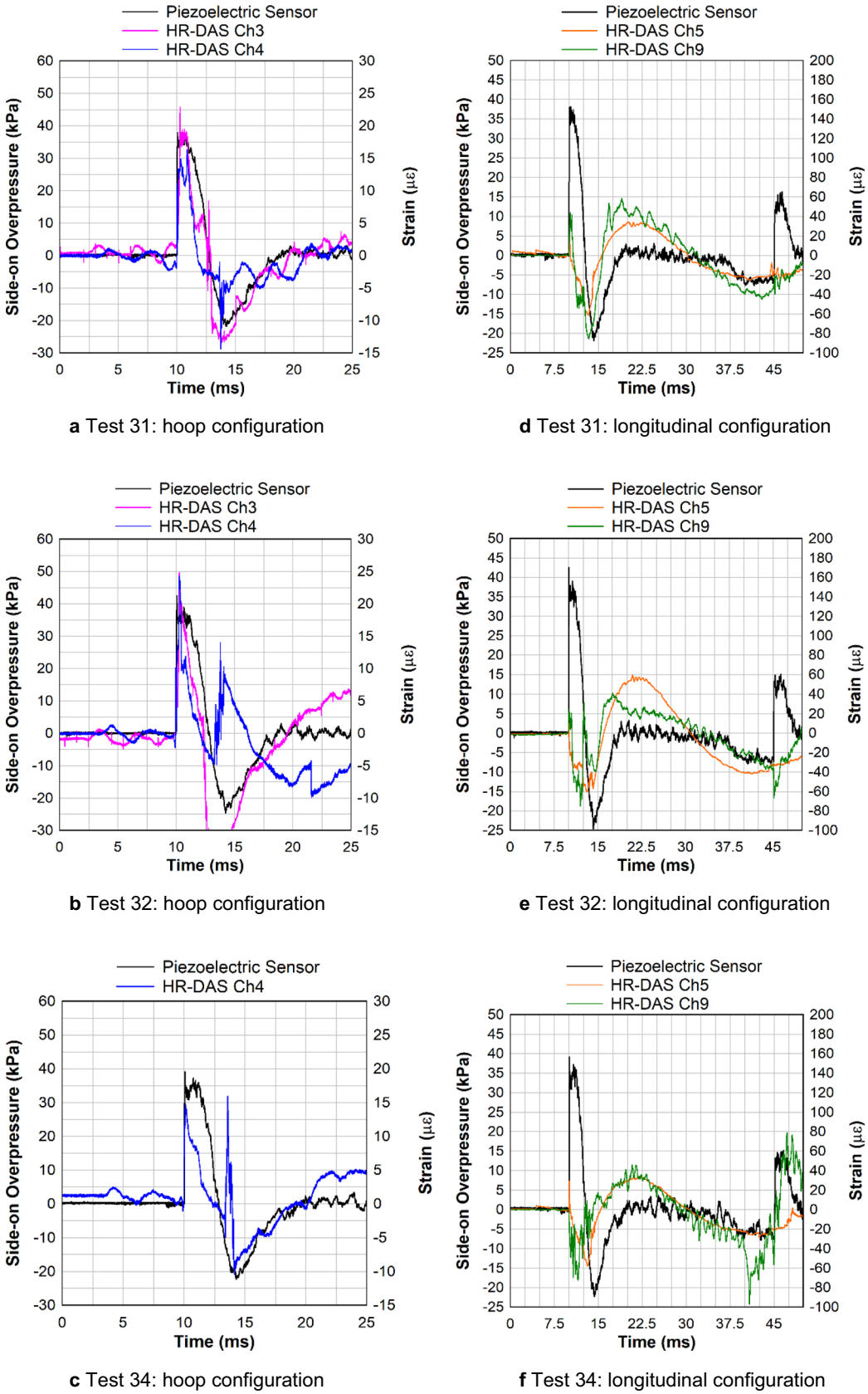

Fig. 13 Overlaid overpressure and strain histories measured by the piezoelectric and HR-DAS sensors arranged in a hoop configuration at channels 3 and 4 (**a**–**c**) and arranged in a longitudinal configuration at channels 5 and 9 (**d**–**f**), displaying poor agreement

Table 7 Strain data captured by HR-DAS sensors (Ch3 and Ch4) subjected to shock waves using 125-μm Mylar diaphragms (Phase B)

Test ID	HR-DAS channel no.	HR-DAS measurements				
		Peak incident strain (με)	Maximum strain (με)	Positive phase duration (ms)	Peak negative strain (με)	Negative phase duration (ms)
31	3	22.9	21.7	2.79	−13.4	7.03
	4	15.1	16.3	2.15	−14.4	9.04
32	3	25.2	25.2	2.39	−20.7	7.16
	4	24.3	24.3	2.13	–	–
34	3	–	–	–	–	–
	4	14.8	14.8	2.48	−10.5	6.42

overpressures, the strain may exceed the fibre's material limits, causing failure in tension or compression, necessitating protective jackets or otherwise.

In addition to these technical considerations, HR-DAS presents potential practical advantages for large-scale blast measurement applications. A single interrogator can support a very large number of sensing points along one fibre, substantially reducing the effective cost per node and providing a sensor that may be more robust and less susceptible to physical damage than discrete pressure transducers.

In this study, HR-DAS measurements demonstrated sensitivity to the adhesive covering used to secure the sensing fibre to the inner shock tube wall (i.e., masking tape vs. duct tape). Generally, better agreement was observed in Phase B tests, both in terms of qualitative waveform agreement and durations, where fibres were secured using double-sided tape topped with duct tape. Despite near-equivalent blast loading conditions (i.e., using 125-μm Mylar diaphragms) and the same hoop orientation, peak strain magnitudes measured in Phase B tests (i.e., $\approx$ 15–25 με) were larger by approximately a factor of three than in Phase A tests (i.e., $\approx$ 5–6 με). This confirms that the HR-DAS measurement is also influenced by the type of adhesive covering used, warranting further investigation.

An important finding from this study relates to the orientation of the DAS sensing fibre with respect to the shock wave propagation. DAS sensors configured in a longitudinal axis (parallel to shock propagation) lacked agreement with pressure histories, suggesting that HR-DAS sensors must be placed orthogonal to the shock propagation direction (i.e., hoop in the case of a shock tube) to generate meaningful side-on blast wave measurements.

Although the resolution of the HR-DAS sensor has improved and is now approaching that of traditional piezoelectric point sensors, the intrinsic length of the sensing fibre (between a reflector pair) limits agreement when oriented in the longitudinal direction. HR-DAS fibres measure net elongation, meaning that if some regions are in tension while others are neutral or in compression, the resulting reading reflects the average strain over the entire gauge length. When the DAS sensors were aligned parallel to the shock propagation inside the shock tube, the fibre experienced localised, incremental loading of varying magnitudes along its length (Fig. 14a), rather than the uniform loading seen in the hoop configuration (Fig. 14b). This also accounts for the longer strain duration measured in the longitudinal orientation, as the shock wave requires additional time to travel along the full length of the sensor.

These findings underscore the limitations associated with the fibre sensing length, L, between respective reflectors when the loading event is dynamic, both spatially and temporally, such as the passage of the shock wave, which can lead to complex and potentially meaningless data. This effect can be reduced or eliminated by substantially reducing the distance L between the reflectors from 15 cm to 1 cm, a distance that better represents a point sensor. These observations also highlight the importance of fibre sensor orientation with respect to the loading event and the scale of the sensing fibre with the dynamic loading time duration.

4.1 Limitations

While this study has confirmed the feasibility of HR-DAS for measuring air blast parameters, several limitations and complexities are deserving of further investigation.

The HR-DAS strain dataset is relatively limited due to the challenges in manually triggering data capture for the HR-DAS system; as such, the repeatability of the sensing method in this case could not be explored. For similar reasons, although a linear trend was observed between peak overpressure and peak strain, only two blast loading conditions were examined in this study, which is not sufficient to confirm the linearity of the sensor response.

A higher pulse repetition rate is also required, as the extreme nature of the blast wave exerts rapid and relatively high strain fluctuations, which can cause the output of the optical interferometer to traverse "multiple fringes". This leads to aliasing issues and potential data loss, preventing

Table 8 The comparison of positive and negative blast wave durations measured by the piezoelectric and HR-DAS sensors (Phase B)

Test ID	HR-DAS channel no.	Shock tube blast loading setup	HR-DAS positive phase duration (ms)	Piezoelectric positive phase duration (ms)	Difference (ms)	% Difference	HR-DAS negative phase duration (ms)	Piezoelectric negative phase duration (ms)	Difference (ms)	% Difference
31	3	125-μm Mylar membrane ($p_{so,av} \approx$ 39 kPa)	2.79	2.71	0.08	3.0%	7.03	6.12	0.91	14.9%
	4		2.15		−0.56	−20.7%	9.04		2.92	47.7%
32	3		2.39	2.78	−0.39	−14.0%	7.16	5.77	1.39	24.1%
	4		2.13		−0.65	−23.4%	–		–	–
34	3			2.84		0.0%	–	6.99		
	4		2.48		−0.36	−12.7%	6.42		−0.57	−8.2%

the system from fully resolving the true strain history of the event. The current 2-μs sampling interval is insufficient to capture the steep rise associated with the shock front, which typically occurs on sub-microsecond timescales. As a result, the peak strain and the initial gradient of the waveform may not be accurately captured, limiting the system's ability to characterise the sharpness and magnitude of the loading event.

Blast wave interaction with the fibre itself should also be acknowledged. Despite efforts to maintain a near-flush mounting, the fibre installation involved mounting the fibre on the inner surface of the shock tube wall (secured with either masking or electrical insulation tape), which will have introduced a small projected area normal to the shock propagation direction. For fibres orientated in the hoop configuration, a bow shock can be expected to have formed at the leading edge of the fibre, which, coupled with differential shock transmission through the tape, will have caused some asymmetric loading on the fibre. For a bare fibre with an outer diameter of 250 μm, and an estimated shock front velocity of 396 m/s (based on Rankine-Hugoniot relations and $p_{so} = 39$ kPa), shock front passage (over the fibre) can be expected to have occurred within approximately 0.63 μs. When considering the increased thickness of the fibre mounting with the tape secured on top (which has a similar thickness to the fibre), the effective crossing time would increase by 2–3 times, or nearly 2 μs. This behaviour should be visible in the rise times of the shock front in the measured strain-time histories. However, due to the upper frequency limit of 250 kHz in these tests and the rapid shock front crossing times described previously, a higher sampling rate would be required to examine this in detail and to assess whether precise flush mounting is necessary to avoid distortion in the measured response.

Between successive tests, all fibre sensor locations were visually inspected to confirm that the adhesive interface remained intact and that the pre-strain condition was maintained. Although this did not adversely affect the current results, some variability in the applied pre-strain cannot be ruled out.

The pressure sensitivity of the fibre to hydrostatic pressure was measured using a Mach–Zehnder interferometer (MZI) setup and a water tank. In this experiment, the sensing arm of the MZI was submerged in water, and an underwater speaker generated controlled hydrostatic pressures. The measured pressure sensitivity of the fibre was −74.5 μrad/(Pa m) (7), which is approximately 40 times lower than the strain sensitivity observed during the shock tube tests using the HR-DAS. This discrepancy may arise from three factors, including asymmetric loading on the fibre during blast exposure, the limitations of applying hydrostatic pressure-based models to blast wave conditions, and simplifications in the

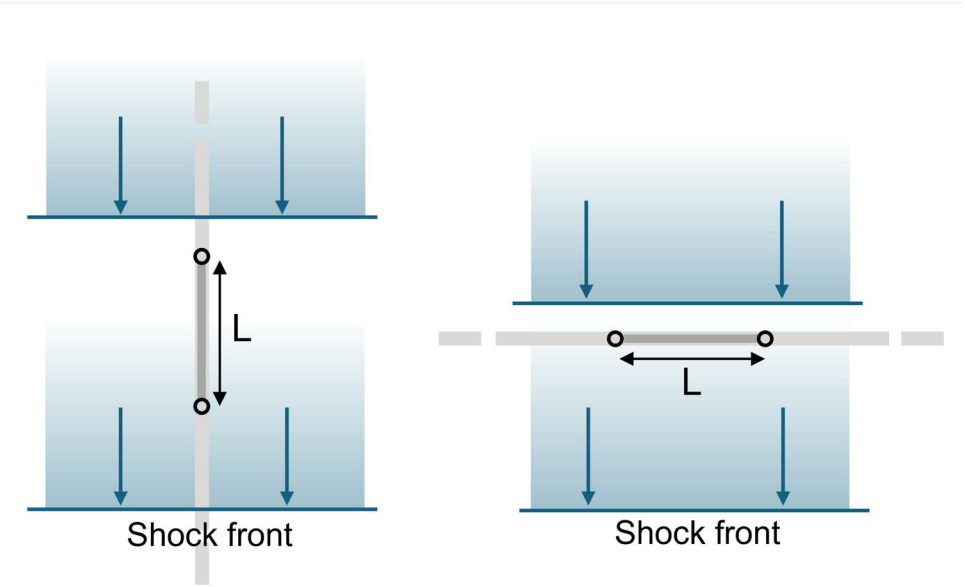

Fig. 14 Differential loading exerted on sensing fibre with length L in "longitudinal" configuration with respect to shock wave propagation (left) in comparison with uniform loading experienced in the "hoop" arrangement (right)

theoretical analysis, such as neglecting pressure wave reflections at the fibre-tape interface:

1. First, cross-sensitivity of the fibre to strain may have influenced the measurements. During shock wave propagation, fibre elongation could occur due to drag forces (if the fibre is not securely attached) or radial expansion of the shock tube. The HR-DAS system cannot distinguish between pressure-induced strain from a blast wave and strain due to mechanical elongations of the shock tube, introducing potential measurement errors.
2. Second, the theoretical framework used to estimate the fibre's pressure sensitivity might not fully account for the behaviour of the fibre under shock loading conditions. While the hydrostatic pressure sensitivity measurement approach is well-established, it may not accurately capture fibre behaviour under a shock wave loading regime. Unlike hydrostatic loading, which is quasi-static with stable material behaviour, shock loading involves rapid, high-pressure events with extreme strain rates and non-equilibrium states [22]. These differences might explain the difference between the hydrostatic and shock loading sensitivities of the fibre, which requires further investigation.
3. A third potential contributor to the observed strain response is rapid temperature change behind the shock front. Estimated post-shock temperature rises of +17.5 °C and +40.9 °C were calculated using Rankine–Hugoniot relations for the 39 kPa and 72 kPa overpressure cases, respectively. These transients occurred over microsecond timescales and are expected to have decayed rapidly. Given the short duration and low thermal conductivity of the fibre and coating, heat transfer into the sensing region is likely to have been minimal. While some thermal expansion may have contributed to the measured strain, the effect is expected to be small.

Given the difference in sensitivity, our comparison between pressure sensor data and HR-DAS focused on qualitative agreement: specifically, the timing and duration of positive and negative strain phases in the HR-DAS signal relative to the overpressure profiles captured by the piezoelectric sensors.

A key limitation of the current setup is the uncertainty regarding the source of the measured strain: whether it arises predominantly from pressure-induced radial loading or mechanical strain in the shock tube wall. Since the HR-DAS fibres were secured to the inner surface of the steel tube with tape, they are inevitably susceptible to structural vibration and strain propagation within the tube wall, analogous to a traditional strain gauge. This mechanical coupling may obscure the distinction between dynamic pressure loading and structural response. Conversely, insufficient adherence may allow the fibre to experience local acceleration or drag effects from the blast winds, introducing further strain unrelated to overpressure. Moreover, the fibre was not directly exposed to the free-field blast wave; instead, the pressure signal was transmitted through a tape layer, which itself may have modified or attenuated the pressure waveform. As such, while the HR-DAS signals qualitatively resemble pressure transients, their attribution to air blast overpressure alone cannot yet be confirmed. A fully decoupled, pressure-isolated mounting method is required in future studies to distinguish true pressure-induced strain from other sources.

Similar challenges have been reported for other optical measurement techniques, such as Photonic Doppler

Velocimetry (PDV), where wall vibration and early structural response can influence the recorded signal. A comparative evaluation of PDV and HR-DAS behaviour under blast loading could therefore provide useful insight in future work.

4.2 Future work

Several areas for future work are proposed to address the limitations identified in this study and to further develop the HR-DAS system for blast diagnostics:

- *Expanded blast loading conditions*—Conduct further tests across a wider range of peak overpressures and positive phase durations to assess the proportionality of the fibre response and support quantitative calibration under varied impulse conditions.
- *Trigger synchronisation*—Automatic triggering and synchronisation between the HR-DAS and conventional pressure sensors will improve repeatability and support direct time-of-arrival comparisons.
- *Improved temporal and spatial resolution*—Increasing the sampling rate of the system will resolve the submicrosecond rise times associated with the shock front and mitigate aliasing and fringe skipping. Reducing the HR-DAS gauge length to 2 cm will help to minimise spatial averaging and improve sensitivity to local strain gradients.
- *Controlled fibre pre-straining*—Developing consistent and quantifiable pre-straining methods for fibre installation will improve sensor repeatability and support calibration efforts.
- *Dynamic calibration*—Refine the theoretical model and establish a calibration approach suitable for the transient and high-strain-rate nature of blast loading.
- *Thermal effect characterisation*—Explore the influence of transient temperature rises on the measured strain through controlled testing and numerical simulation.
- *Decoupled sensing strategy*—To reduce uncertainty and better characterise the relative contributions of dynamic pressure loading and structural deformation, future experiments will employ a differential HR-DAS configuration. This will involve mounting one fibre to the internal surface of the shock tube, where it will be subjected to both blast pressure-induced strain and potential wall strain, and a second fibre to the external surface, where strain is expected to arise solely from shock tube deformation. In addition, synchronised electrical strain gauges will be installed adjacent to selected fibre locations to provide an independent reference for the structural strain history. This combined approach is expected to improve confidence in the interpretation of HR-DAS data and support the development of future calibration strategies.

5 Conclusions

In this study, shock tube experiments examined the capability of HR-DAS sensors to capture strain responses associated with side-on blast wave overpressure histories through comparison with a reference piezoelectric pressure sensor, specifically examining the effects of sensor orientation (i.e., hoop or longitudinal) and the influence of two different sensor (fibre) adhesive coverings.

Results confirmed that the HR-DAS system can measure strain-time profiles when subjected to blast wave loading with good qualitative agreement to overpressure histories. The results revealed strong agreement between the HR-DAS and piezoelectric sensor measurements when HR-DAS sensors were mounted perpendicular to the blast wave propagation, validating the system's efficacy under uniform loading conditions. However, discrepancies were observed for sensors aligned parallel to the wave direction, highlighting the limitations of the fibre sensing length and orientation when subjected to dynamic, spatially varying loading scenarios. These findings emphasise the importance of sensor placement and configuration for distributed pressure analysis.

These results and recommendations highlight an interesting opportunity to develop a novel blast pressure instrumentation method. This method, which is small in size and relatively low cost, enables multiple measurement points from a single optical fibre and addresses several limitations with conventional pressure instrumentation methods. These proof-of-concept findings will be of direct interest to defence stakeholders and researchers in the blast protection and blast injury research fields who are undertaking physical blast tests.

Acknowledgements The research leading to these results received funding from The Royal Society under Grant Agreement No. RGS\R1\231115.

Funding The authors have no relevant financial or non-financial interests to disclose.

Data availability The data supporting the findings of this study are not available online due to the large volume and size of the files. Datasets generated during the current study are available from the corresponding author on reasonable request.

Declarations

Conflict of interest The authors have no conflict of interest to declare that are relevant to the content of this article.

References

1. Friedlander, F.G.: The diffraction of sound pulses. II. Diffraction by an infinite wedge. Proc. R. Soc. Lond. A Math. Phys. Eng. Sci. **186**(1006), 344–351 (1946). https://doi.org/10.1098/rspa.1946.0046
2. Eaton, W.P., Smith, J.H.: Micromachined pressure sensors: review and recent developments. Smart Mater. Struct. **6**(5), 530–539 (1997). https://doi.org/10.1088/0964-1726/6/5/004
3. Needham, C.E., Ritzel, D., Rule, G.T., Wiri, S., Young, L.: Blast testing issues and TBI: experimental models that lead to wrong conclusions. Front. Neurol. **6**, 72 (2015). https://doi.org/10.3389/fneur.2015.00072
4. Watson, S., Macpherson, W.N., Barton, J.S., Jones, J.D.C., Tyas, A., Pichugin, A.V., Hindle, A., Parkes, W., Dunare, C., Stevenson, T.: Investigation of shock waves in explosive blasts using fibre optic pressure sensors. Meas. Sci. Technol. **17**(6), 1337–1342 (2006). https://doi.org/10.1088/0957-0233/17/6/008
5. MacPherson, W.N., Gander, M.J., Barton, J.S., Jones, J.D.C., Owen, C.L., Watson, A.J., Allen, R.M.: Blast-pressure measurement with a high-bandwidth fibre optic pressure sensor. Meas. Sci. Technol. **11**, 95–102 (2000). https://doi.org/10.1088/0957-0233/11/2/302
6. Zou, X., Wu, N., Tian, Y., Zhang, Y., Fitek, J., Maffeo, M., Niezrecki, C., Chen, J., Wang, X.: Ultrafast Fabry-Perot fiber-optic pressure sensors for multimedia blast event measurements. Appl. Opt. **52**(6), 1248–1255 (2013). https://doi.org/10.1364/AO.52.001248
7. Parkes, W., Djakov, V., Barton, J.S., Watson, S., MacPherson, W.N., Stevenson, J.T.M., Dunare, C.C.: Design and fabrication of dielectric diaphragm pressure sensors for applications to shock wave measurement in air. J. Micromech. Microeng. **17**(7), 1334–1342 (2007). https://doi.org/10.1088/0960-1317/17/7/016
8. Pooley, J., Price, E., Ferguson, J.W., Ibsen, M.: Detonation velocity measurements with uniform fibre Bragg gratings. Opt. Express **27**(16), 23464–23473 (2019). https://doi.org/10.1364/OE.27.023464
9. Zhang, L., Yang, Z., Szostkiewicz, L., Markiewicz, K., Mikhailov, S., Geernaert, T., Rochat, E., Thévenaz, L.: Long-distance distributed pressure sensing based on frequency-scanned phase-sensitive optical time-domain reflectometry. Opt. Express **29**(13), 20487–20498 (2021). https://doi.org/10.1364/OE.425501
10. Mikhailov, S., Zhang, L., Geernaert, T., Berghmans, F., Thévenaz, L.: Distributed hydrostatic pressure measurement using phase-OTDR in a highly birefringent photonic crystal fiber. J. Lightwave Technol. **37**(18), 4496–4500 (2019). https://doi.org/10.1109/JLT.2019.2904756
11. Masoudi, A., Belal, M., Newson, T.P.: Distributed optical fibre audible frequency sensor. Proceedings of 23rd International Conference on Optical Fibre Sensors, SPIE, vol. 9157, 91753T (2014). https://doi.org/10.1117/12.2058484
12. Muggleton, J.M., Hunt, R., Rustighi, E., Lees, G., Pearce, A.: Gas pipeline leak noise measurements using optical fibre distributed acoustic sensing. J. Nat. Gas Sci. Eng. **78**, 103293 (2020). https://doi.org/10.1016/j.jngse.2020.103293
13. Owen, A., Duckworth, G., Worsley, J.: OptaSense: fibre optic distributed acoustic sensing for border monitoring. Proceedings 2012 European Intelligence and Security Informatics Conference (EISIC), pp. 362–364. IEEE (2012). https://doi.org/10.1109/EISIC.2012.59
14. Matthaiou, I., Masoudi, A., Araki, E., Kodaira, S., Modafferi, S., Brambilla, G.: Classification of images derived from submarine fibre optic sensing: detecting broadband seismic activity from hydroacoustic signals. Geophys. J. Int. **240**(1), 483–501 (2024). https://doi.org/10.1093/gji/ggae400
15. Milne, D., Masoudi, A., Ferro, E., Watson, G., Le Pen, L.: An analysis of railway track behaviour based on distributed optical fibre acoustic sensing. Mech. Syst. Signal Process. **142**, 106769 (2020). https://doi.org/10.1016/j.ymssp.2020.106769
16. Hartog, A.H.: An Introduction to Distributed Optical Fibre Sensors. CRC Press, Boca Raton (2017). https://doi.org/10.1201/9781315119014
17. Masoudi, A., Lee, T., Beresna, M., Brambilla, G.: 10-cm spatial resolution distributed acoustic sensor based on an ultra-low-loss enhanced backscattering fiber. Opt. Continuum **1**(9), 2002–2010 (2022). https://doi.org/10.1364/OPTCON.468673
18. Lee, T., Beresna, M., Masoudi, A., Brambilla, G.: Enhanced-backscattering and enhanced-backreflection fibers for distributed optical fiber sensors. J. Lightwave Technol. **41**(13), 4051–4064 (2023). https://doi.org/10.1109/JLT.2023.3281136
19. Hocker, G.B.: Fiber-optic sensing of pressure and temperature. Appl. Opt. **18**(9), 1445–1448 (1979). https://doi.org/10.1364/AO.18.001445
20. Budiansky, B., Drucker, D.C., Kino, G.S., Rice, J.R.: Pressure sensitivity of a clad optical fiber. Appl. Opt. **18**(24), 4085–4088 (1979). https://doi.org/10.1364/AO.18.004085
21. Bloodworth-Race, S., Critchley, R., Hazael, R., Peare, A., Temple, T.: Testing the blast response of foam inserts for helmets. Heliyon **7**(5), e06990 (2021). https://doi.org/10.1016/j.heliyon.2021.e06990
22. Sikka, S.K.: Behaviour of materials under shock loading conditions. Bull. Mater. Sci. **15**, 35–46 (1992). https://doi.org/10.1007/BF02745215